BIOCHEMISTRY
including biophysical chemistry & molecular biology

Article

pubs.acs.org/biochemistry

# Characterization of the Interface of the Bone Marrow Stromal Cell Antigen 2−Vpu Protein Complex via Computational Chemistry

Jinming Zhou,*[,†] Zhixin Zhang,[†] Zeyun Mi,[†] Xin Wang,[†] Quan Zhang,[†] Xiaoyu Li,[†] Chen Liang,[‡,§] and Shan Cen*[,†]

[†]Institute of Medicinal Biotechnology, Chinese Academy of Medical Science, Beijing, China

[‡]Lady Davis Institute for Medical Research and McGill AIDS Centre, Jewish General Hospital, Montreal, Quebec, Canada

[§]Microbiology and Immunology, McGill University, Montreal, Quebec, Canada

Supporting Information

**ABSTRACT:** Bone marrow stromal cell antigen 2 (BST-2) inhibits the release of enveloped viruses from the cell surface. Various viral counter measures have been discovered, which allow viruses to escape BST-2 restriction. Human immunodeficiency virus type 1 (HIV-1) encodes viral protein U (Vpu) that interacts with BST-2 through their transmembrane domains and causes the downregulation of cell surface BST-2. In this study, we used a computer modeling method to establish a molecular model to investigate the binding interface of the transmembrane domains of BST-2 and Vpu. The model predicts that the interface is composed of Vpu residues I6, A10, A14, A18, V25, and W22 and BST-2 residues L23, I26, V30, I34, V35, L41, I42, and T45. Introduction of mutations that have been previously reported to disrupt the Vpu−BST-2 interaction led to a calculated higher binding free energy (MMGBSA), which supports our molecular model. A pharmacophore was also generated on the basis of this model. Our results provide a precise model that predicts the detailed interaction occurring between the transmembrane domains of Vpu and BST-2 and should facilitate the design of anti-HIV agents that are able to disrupt this interaction.

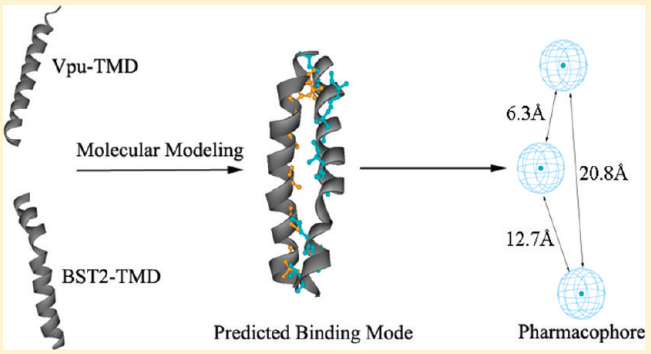


Bone marrow stromal cell antigen 2 (BST-2, also known as tetherin, CD317, or HM1.24) is an integral membrane protein with a unique topology. BST-2 bears a short cytoplasmic N-terminal region, a transmembrane domain (TMD), a disulfide-linked coiled coil ectodomain, and a glycophosphatidylinositol lipid (GPI) anchor at its C-terminus.[1] The antiviral activity of BST-2 was first reported for its ability to block the release of progeny HIV-1 particles from the cell surface in the absence of the viral protein, Vpu. Electron microscopy revealed the accumulation of viral particles at the surface of BST-2-expressing cells, with BST-2 found between the tethered viral particles and the plasma membrane, suggesting a direct role of BST-2 in blocking virus release.[2] Furthermore, BST-2 may diminish the infectivity of released HIV-1 particles.[3] In addition to HIV-1, a wide range of enveloped viruses have been reported to be subject to BST-2 restriction, including other retroviruses, filoviruses, arenaviruses, orthomyxoviruses, and rhabdoviruses.[1]

Viruses have evolved various measures to counteract BST-2. In the case of HIV-1, Vpu serves as the BST-2 antagonist.[2,4,5] Vpu is an 81-amino acid, type I integral membrane phosphoprotein. It has an N-terminal transmembrane domain and a cytoplasmic domain.[6] It has been long known that in addition to downregulating CD4 at the endoplasmic reticulum, Vpu also promotes HIV-1 release. Recent evidence suggests that Vpu downregulates BST-2 from the cell surface and removes BST-2 from the sites of virus budding, thereby overcoming the anti-HIV activity of BST-2.[1,2,4,5] This downregulation may result from several actions of Vpu,[5,7−11] such as sequestration of BST-2 at the perinuclear region, lysosome-dependent degradation of BST-2 through recruiting the β-TrCP E3 ligase complex with the resulting addition of ubiquitin to the cytoplasmic tail of BST-2, and redirecting BST-2 intracellular trafficking. It is noted that all of these Vpu activities depend on the ability of Vpu to interact with BST-2 through the transmembrane domains of these two proteins,[7−10,12−18] while the precise mechanism through which Vpu antagonizes BST-2 requires further elucidation.[12,13]

Indeed, sequence disparity in the transmembrane domains of human and monkey BST-2 renders monkey BST-2 resistant to HIV-1 Vpu antagonization.[7,9] Detailed mutagenesis studies further revealed that mutations in the BST-2 transmembrane domain (for example, amino acid substitutions of L22, L23, G25, I26, V30, I33, I34, I36, L37, L41, and T4) resulted in a Vpu-resistant phenotype.[10,13] Interestingly, these residues tend

**Received:** October 19, 2011
**Revised:** January 12, 2012
**Published:** January 17, 2012

   dx.doi.org/10.1021/bi2015986 | *Biochemistry* 2012, 51, 1288−1296

to be located at the same side of a helical structure predicted in an initial molecular modeling of the BST-2 transmembrane domain.[10,13] Similarly, mutation of amino acids A14, A18, and W22 abrogates the counteraction of Vpu against BST-2, and they also occupy the same side of the helical structure in the Vpu transmembrane domain.[8,19] These residues may therefore constitute the interface for the Vpu−BST-2 interaction.[8,13]

Computer modeling is routinely used to investigate the interactions of biological molecules in membranes. For example, Yin et al. designed the anti-aIIb and anti-av peptides to interfere with the homointeraction of aIIb or av TMD in membranes using a computed helical antimembrane protein (CHAMP) method;[20,21] Rizzo et al. simulated the interaction of T20 and GP-41 utilizing molecular modeling to verify the resistance mechanism of HIVgp41 viral entry inhibitor T20.[22] Computer modeling of BST2-TM dimer or Vpu-TM dimer has also been reported by several groups,[23−27] and the computational modeling for the interaction of the TMD of Vpu or Vpu-A18H and BST-2 has been done, predicting the A18H mutant may lead to an interaction less stable than that obtained with wild-type Vpu.[28] However, a precise molecular model for the interaction of BST-2 and Vpu remains to be determined to more clearly understand the mechanism of Vpu antagonism and provide a structural basis for rational drug design.[13] In this work, we built and evaluated an interaction model of BST-2 and Vpu at the atomic level, using molecular docking and molecular dynamics. The binding model is consistent with biological assay data and the recent results using NMR,[29] and such a model should lead to an improved understanding of the molecular recognition between BST-2 and Vpu, thereby promoting rational design of drugs that would target the BST-2−Vpu complex.

## METHODS

**Construction of the Initial Structural Models.** The initial structures for the BST2-TM dimer peptide (residues 21−48, termed BST2-TM) and Vpu-TM dimer peptide (residues 6−21, termed Vpu-TM) were generated as $\alpha$-helical secondary structures using Discovery Studio 2.5. In particular, the constructed peptides were capped with an acetyl group at the N-terminus and an $NH_2$ group at the C-terminus. These initial structures were then embedded into an explicit DOPC lipid membrane including explicit solvent using Discovery Studio 2.5 to generate the input structures for the later molecular dynamics simulation in membranes. The membrane was generated using the VMD software suite,[30] followed by the 3 ns pre-equilibrium in AMBER (University of California, San Francisco, CA). The partial charges on the DOPC monomer were calculated by fully reproducible ab initio electronic structure computations with Gaussian 09 (Gaussian, Inc., Wallingford, CT) using the Hartree−Fock self-consistent field (HF-SCF) with the 6-31G* basis set after optimizing with DFT-B3LYP and successively with HF-SCF at the 6-31G* level. The partial charges were then extracted following the RESP protocol with the ANTECHAMBER program of the AMBER suite. The molecular dynamics (MD) simulations were performed using AMBER version 10, all-atom parm94 force fields, particle mesh Ewald summation, the SHAKE algorithm, and a time step of 2 fs. The systems were minimized using the steepest decent method, followed by the conjugate gradient method to remove the bad contacts. An equilibrium period of 120 ps was allowed before the MD simulations commenced. The 10 ns MD simulations were conducted in the NPT ensemble for both BST2-TM and Vpu-TM, and the constant temperature (310 K) and constant pressure (1 bar) were maintained using the Langevin piston coupling algorithm.[31] After the simulation had been completed, a cluster analysis was performed for the snapshots taken from the period of 3−10 ns, which amounts to 7000 snapshots for each simulation. Conformation clustering was performed with a radius of 2 Å using the "Kclust" module implemented in the MMTSB software suite (The Scripps Research Institute). The obtained representative structure of the largest cluster family would be served as the representative conformation for the corresponding peptide.

**Construction of the Binding Mode for the BST-TM−Vpu-TM Complex.** The initial binding modes for the BST2-TM−Vpu-TM complex were generated through molecular docking using Molecular Operating Environment (MOE, Chemical Computing Group Inc., Montreal, QC) version 2009.10. In general, docking was performed through the "DOCK" module in MOE using the alpha triangle placement method. Refinement of the docked poses was conducted using the force field refinement scheme and scored using both the affinity dG and London dG scoring systems. Thirty poses were returned as the results of docking, for which the cluster analysis was further performed with a radius of 10 Å in the MMTSB software suite.

**Evaluation of the Binding Mode and Calculations of Binding Energy.** To further verify the most favorable binding mode, we estimated the binding free energy using the single-trajectory molecular mechanics generalized Born surface area (MM-GBSA) method[32] for each representative structure. In brief, the representative structure was inserted into the built membrane, and a corresponding simulation was performed as previously mentioned; the snapshots from the period of 6−9 ns for each simulation were output as ensembles for the free binding energy estimation. The overall binding free energy between the peptides was calculated with the following equation:

$$\begin{aligned}\Delta G_{\text{bind}} &= \Delta G_{\text{gas}} + \Delta G_{\text{solvation}} \\ &= \Delta E_{\text{ele}} + \Delta E_{\text{vdW}} + \Delta E_{\text{int}} + \Delta G_{\text{polar}} \\ &\quad + \Delta G_{\text{nonpolar}}\end{aligned}$$

$\Delta G_{\text{gas}}$ was obtained by summing the molecular mechanical (MM) internal ($\Delta E_{\text{int}}$), electrostatic ($\Delta E_{\text{ele}}$), and van der Waals ($\Delta E_{\text{vdw}}$) energies. $\Delta G_{\text{solvation}}$ equals the sum of polar ($\Delta G_{\text{polar}}$) and nonpolar ($\Delta G_{\text{nonpolar}}$) contributions. $\Delta G_{\text{polar}}$ was calculated by the GB model using the parameters developed by Onufriev et al.,[33] and the values of the interior and the exterior dielectric constants were set to 1 and 80, respectively. $\Delta G_{\text{nonpolar}}$ was calculated from the solvent accessible surface area determined by the LCPO method:[34] $\Delta G_{\text{nonpolar}} = 0.0072 \times \text{SASA}$. No additional entropic terms were added. It should be emphasized that all MD simulations employed explicit solvent and explicit lipid; thus, the ensemble of conformations is representative of that generated in the condensed phase. The representative conformation with the favorable binding free energy would be treated as the favorable binding mode. Next, several mutants that may cause the elimination or relief of the interaction between Vpu and BST-2 were examined through the MD simulation and the free energy estimation using the MMGBSA method. In particular, single-point mutations were performed using DS 2.5 based on the obtained favorable binding mode to

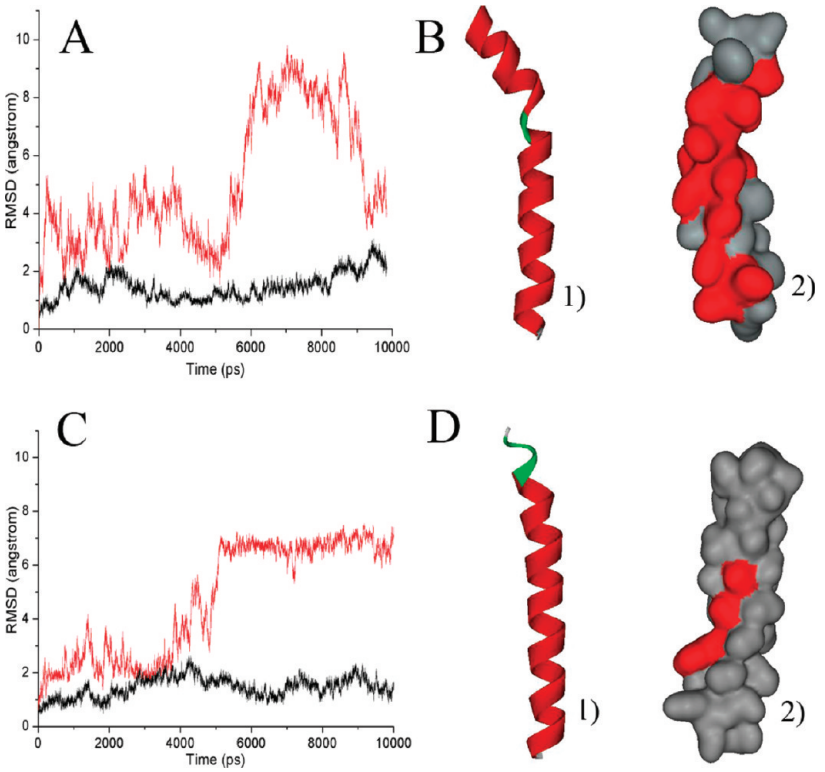


**Figure 1.** Results of the simulation for Vpu-TM and BST2-TM in a DOPC membrane. The rmsd was calculated by the superimposition of the C$\alpha$ atoms between the instantaneous MD structure and initial model, and the representative structure was generated by cluster analysis of 7000 snapshots taken from the period of 3−10 ns of the MD simulations in the membrane. (A) rmsd analysis of the BST2-TM simulation (red line, simulation in aqueous medium; black line, simulation in the membrane). (B) Representative structure for the BST2-TM simulation. (C) rmsd analysis for the Vpu-TM simulation (red line, simulation in aqueous medium; black line, simulation in the membrane). (D) Representative structure for the Vpu-TM simulation.

make sure that the mutant complex structures were at the exact position in the membrane. The MD simulation as well as the free energy calculation was conducted as previously described.

## RESULTS AND DISCUSSION

**Conformational Analysis of BST2-TM and Vpu-TM in a DOPC Membrane.** Because the three-dimensional (3D) structure of BST2-TM has not yet been resolved, we built a 3D model of BST2-TM through molecular modeling, as previously described. Notably, the secondary structure of BST2-TM is thought to adopt a helix conformation, as does the membrane domain of other proteins similar in sequence to BST2-TM.[35] Therefore, the $\alpha$-helical conformation was chosen herein as the initial conformation of the peptide. To investigate further the conformation of BST2-TM in membranes, the simulation in a DOPC membrane was performed, and a simulation in aqueous medium was also conducted as a comparison using the same initial structure. As shown in Figure 1A, the values of the root-mean-square deviation (rmsd) between the instantaneous MD structure and initial model for the simulation in membrane are <3 Å, while those for the simulation in aqueous are largely fluctuating between 2 and 10 Å. This indicates that BST2-TM exhibits a much more stable conformation in the membrane than in aqueous medium. Next, we performed cluster analysis to identify the most favorable conformation using the 7000 snapshots taken from the period of 3−10 ns of the MD simulations in the membrane. As a result, two families were obtained with a radius of 2 Å, and the largest family was dominant, with 5746 members. The representative structure for the largest family was defined by the snapshot that is closest to the average structure of that family and is shown in Figure 1B. To our surprise, a turn was generated at position G38, which splits the peptide into two helices, and resulted in a very stable conformation during simulations. Consistent with this result, a similar conformation of BST2-TM was reported in a molecular modeling study published recently during preparation of this work.[10] Whether the turn is involved in promoting the antivirus of BST-2 or takes part in the interaction between BST-2 and Vpu remains unknown.

Similar simulations were performed for Vpu-TM in the membrane and aqueous medium, and the results are shown in Figure 1C,D. rmsd analysis results are comparable to that of BST2-TM, which indicates that Vpu-TM has a much more stable conformation in the membrane than that in aqueous medium. Cluster analysis for the Vpu-TM simulation was also conducted, and one family was obtained with a radius of 2 Å. The representative structure of the family is shown in Figure 1D. Unlike BST2-TM, Vpu-TM kept an entire single-helix conformation during the simulation. As the three-dimensional structure of Vpu-TM has been reported, we compared the representative structure with the NMR structure (Protein Data Bank entry 1PI7)[19] through the alignment of the C$\alpha$ atoms of the structures, and the results are shown in Figure S2 of the Supporting Information. The modeling structure and the experimental structure (residues 7−25) superimpose with an rmsd of 0.89 Å. Thus, starting from the structure built in DS,


dx.doi.org/10.1021/bi2015986 | *Biochemistry* 2012, 51, 1288−1296

**Table 1. Docking Results of Vpu-TM and BST2-TM[a]**

| rank | affinity dG | cluster | rank | affinity dG | cluster | rank | affinity dG | cluster |
|---|---|---|---|---|---|---|---|---|
| Top1 | −5.74 | 1 | Top11 | −4.13 | 2 | Top21 | −3.14 | 1 |
| Top2 | −5.47 | 3 | Top12 | −3.92 | 1 | Top22 | −2.93 | 2 |
| Top3 | −5.16 | 2 | Top13 | −3.87 | 1 | Top23 | −2.92 | 2 |
| Top4 | −5.14 | 1 | Top14 | −3.87 | 1 | Top24 | −2.8 | 1 |
| Top5 | −5.11 | 2 | Top15 | −3.62 | 2 | Top25 | −2.64 | 2 |
| Top6 | −4.97 | 2 | Top16 | −3.41 | 4 | Top26 | −2.62 | 3 |
| Top7 | −4.59 | 2 | Top17 | −3.39 | 4 | Top27 | −2.47 | 2 |
| Top8 | −4.45 | 2 | Top18 | −3.2 | 1 | Top28 | −2.45 | 1 |
| Top9 | −4.26 | 2 | Top19 | −3.15 | 3 | Top29 | −2.33 | 3 |
| Top10 | −4.23 | 1 | Top20 | −3.14 | 2 | Top30 | −2.14 | 5 |

[a]Both affinity dG and London dG scoring were used to evaluate the docked poses; the ranking number was assigned according to the Affinity dG value.

we have obtained a high accuracy in predicting the structure of Vpu-TM, suggesting that our simulation design is reasonable.

It was reported that amino acid residues L22, L23, G25, I26, V30, I33, I34, I36, L37, L41, and T45 across the BST2-TM might be involved in the interaction between Vpu and BST-2.[10,13] All of these residues are marked in the modeling structure shown in Figure 1. Similar to the results in previous reports,[13] most of these residues also are located on the same side of our structural model (Figure 1B, 2). Furthermore, residues A14, A18, and W22 in Vpu-TM, all of which are critical for the interaction between Vpu and BST-2,[8] are on the same face of our simulation peptide model (Figure1D, 2).

The parameters we used here for the DOPC lipid are from the work of ROSSO,[36] and the partial charges were calculated using the Hartree−Fock self-consistent field (HF-SCF) with the 6-31G* rather than the 3-21g* basis set. Actually, the POPC (palmitoyloleoylphosphatidylcholine) membrane was more prevalent than the DOPC membrane in the recent reports of the simulations of the membrane protein because POPC is the most abundant lipid in animal cells. Therefore, an inspection of whether the diversity of lipids present in the plasma membrane may influence the results of the simulation is strongly recommended; the simulations of BST2-TM and Vpu-TM in POPC[37] were performed as a comparison, and the results (Figure S3 of the Supporting Information) are comparable to those reported in the DOPC membrane. On the other hand, the effects of the simulation time were also inspected. As a 10 ns long simulation may be too short for peptides to generate the final satisfied conformation, a subsequent simulation for BST2-TM in the lipid membrane was performed to determine if the conformation is converged in the previous simulation. The results shown in Figure S4 of the Supporting Information indicate that the rmsds between the representative structures at 10−20, 20−30, 30−40, or 40−50 ns are quite similar to that at 3−7 ns, with the rmsds being <1.0 Å.

**Mode of Binding of Vpu-TM and BST2-TM.** To further investigate the interaction between Vpu-TM and BST2-TM, we performed a molecular docking using the representative structures generated in molecular dynamic simulations as the respective structure of the receptor (BST2-TM) and ligand (Vpu-TM). The docking was conducted using MOE, and the results are reported in Table 1. The top 30 poses ranked by affinity dG were output and were further clustered into five families with a radius of 15 Å. The families have 13, 10, 4, 2, and 1 member(s). Notably, we found that the representative complex structure of the first three most populated families is Top1 (the representative for cluster 2), Top2 (the representative for cluster 1), and Top3 (the representative for cluster 3) in Table 2, respectively. The structures are shown in Figure 2 and differed in their mode of binding. Briefly, BST2-TM and Vpu-TM adopt the antiparallel binding mode for the Top1 complex structure (affinity dG of −5.74, termed binding mode 1), and the $\alpha$-helical secondary structure of residues 2−8 of the Vpu-TM peptide is distorted to some degree as a result of the force field refinement; they adopt a transplacement antiparallel binding mode for the Top2 complex structure (affinity dG of −5.47, termed binding mode 2) and a parallel binding mode for the Top3 complex (affinity dG of −5.16, termed binding mode 3).

**Table 2. Binding Free Energy Evaluation for the Three Binding Modes from the Docking Results**

| binding mode | $\Delta G_{gas}$ | $\Delta\Delta G_{gas}$ | $\Delta G_{bind}$ | $\Delta\Delta G_{bind}$ |
|---|---|---|---|---|
| binding mode 1 | −69.09 ± 3.95 | 0.00 | −47.01 ± 3.23 | 0.00 |
| binding mode 2 | −66.32 ± 5.42 | 2.77 | −39.12 ± 3.08 | 7.89 |
| binding mode 3 | −44.32 ± 4.26 | 24.77 | −46.39 ± 2.85 | 0.62 |

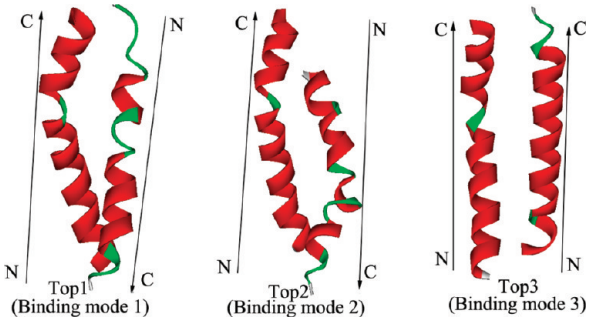


**Figure 2.** Topology of binding modes derived from the docking results. The docking job was conducted using MOE. Top1, Top2, and Top3 docking poses belong to the representative structures of the three most populated families, which are termed binging mode 1, binding mode 2, and binding mode 3, respectively.

The docking job described above and its subsequent refinement were performed in vacuum, and the complex structure obtained might differ from that in the membrane. We next performed an MD simulation starting from the separate representative complex structure in the membrane. As shown in Figure 3, the rmsds between the instantaneous MD structure


dx.doi.org/10.1021/bi2015986 | Biochemistry 2012, 51, 1288−1296

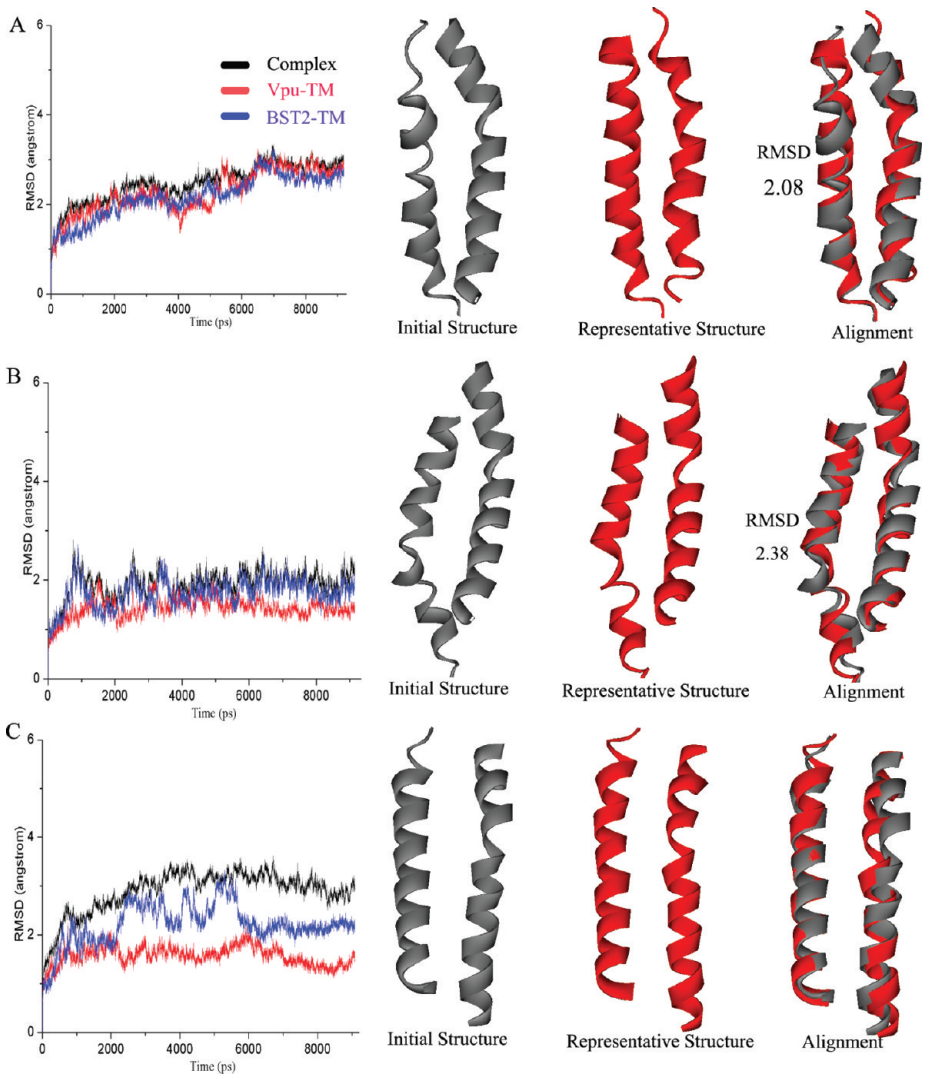


**Figure 3.** Results of molecular dynamics simulations of three docked complex structures. rmsds were calculated by the superimposion of the C$\alpha$ atoms between the instantaneous MD structure and initial model, and the representative structure was generated by cluster analysis. The alignment between the representative structure and initial structure was conducted in DS. (A) Results of analysis of the binding mode 1 simulation (the initial structure was derived from the Top1 docking pose). (B) Results of analysis of the binding mode 2 simulation (the initial structure was derived from the Top2 docking pose). (C) Results of the analysis of the binding mode 3 simulation (the initial structure was derived from the Top3 docking pose).

and the initial model for the simulation in the membrane are <3 Å for all three simulations, which indicates that there is little deviation from the initial structure during the simulation. The representative structure for the snapshot from the period of 3−10 ns of each MD simulation was generated through cluster analysis, and there is one family obtained for all three simulations with a cluster radius of 2 Å. Next, we aligned the initial structure and the representative structure of each simulation (shown in Figure 3). The fitting rmsd values (all <2.5 Å) indicate that the structures fit well. Notably, for the binding mode 1 simulation, the distorted helix structure of residues 2−8 of Vpu was restored during simulation compared to the initial structure.

The binding free energy for each binding mode was calculated using MMGBSA for a further evaluation, and the results are listed in Table 2. Binding mode 1 was identified as the most favorable mode with a calculated binding free energy of −47.01 kcal/mol, being more favorable than binding mode 2 or binding mode 3 by either 7.89 or 0.62 kcal/mol, respectively. Because both BST2-TM and Vpu-TM were buried in the membrane during the simulations, it would be reasonable that the binding modes are evaluated without the consideration of a solvation effect. Accordingly, the free energy without the solvent effect ($\Delta G_{gas}$) of binding mode 1 is ∼2.77 and ∼24.77 kcal/mol more favorable than those of binding modes 2 and 3, respectively. All analysis described above indicates that binding mode 1 is the most favorable binding mode of the three.

BST-2 is a type II integral membrane protein, with the N-terminus in the cytoplasm and the C-terminus in extracellular space. On the other hand, Vpu is a type I integral membrane protein with a topology opposite that of BST-2, with the N-terminus in extracellular space and the C-terminus in the cytoplasm.[6] Therefore, considering the different topologies of BST-2 and Vpu, a putative mode of BST-2 and Vpu was proposed, in which their transmembrane domains should interact in the membrane via an antiparallel binding mode,[13] which is consistent with binding mode 1 in our results. Recently, an NMR study for the interaction of Vpu and BST-2


dx.doi.org/10.1021/bi2015986 | *Biochemistry* 2012, 51, 1288−1296

also showed an antiparallel binding mode of BST2-TM and Vpu-TM.[29]

Next, we compared the residues at the binding interface of binding mode 1 (Figure 4) with the critical residues for the

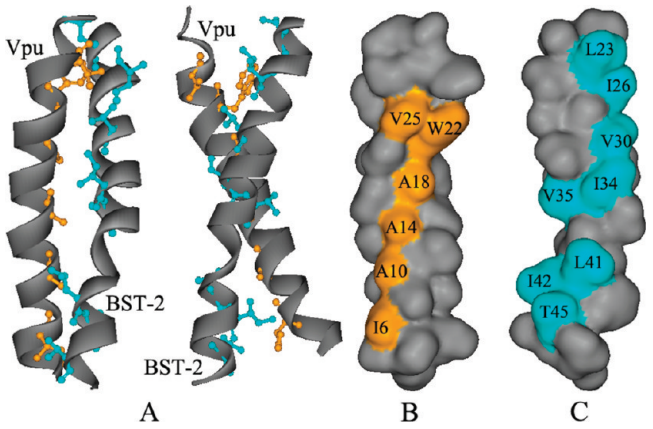


**Figure 4.** Binding mode for the BST2-TM–Vpu-TM complex. (A) Overall view of the binding mode (helix as a gray ribbon and interaction residues as sticks). (B) Interface of Vpu-TM (orange surface). (C) Interface of BST2-TM (cyan surface).

BST-2–Vpu interaction derived from biochemical data. The results are listed in Table 3 and shown in Figure 4. The analysis

**Table 3. Comparison of the Interface Residues Derived from Binding Mode Calculations and Biological Data**

| | Vpu-TM | BST2-TM |
|---|---|---|
| bioassay data | A14, A18, W22, I24, V25 | L22, L23, I26, V30, I33, I34, V35, I36, L37, G38, V39, P40, L41, I42, T45 |
| binding mode 1 interface | I6, A14, I17, A18, V21, W22, V25, Y29 | L23, I26, V30, I34, V35, P40, L41, I42, T45 |

that predicts binding mode 1 indicates that the two peptides interact mainly via hydrophobic interactions, and the binding mode is quite consistent with experimental facts. Notably, residues A14, A18, and W22 at the interface of the Vpu-TM peptide are consistent with the recent mutational studies by Neil et al.,[8] and residues L23, I26, V30, I34, V35, G38, P40, L41, I42, and T45 at the interface of the BST2-TM peptide also are consistent with the bioassay results of the previous reports.[9,10,13] The inconsistent residues, I24 of Vpu-TM and L22, I33, I36, L37, and V39 of BST2-TM, were found at adjacent positions of the interface residues, which might affect the conformation of the interface residues when such a residue is mutated and thereby interfere with the interaction between Vpu and BST-2. Interestingly, besides the reported residues, residues I6, I17, and V21 of Vpu-TM were found to participate in the interaction with BST2-TM.

**Mutant Analysis via Molecular Simulation.** We further investigated which mutants might abolish the interaction between Vpu and BST-2 using MD simulation. Cluster analysis was also performed to generate the representative complex structure of the largest family during the simulation. For all the mutant complexes, the conformation of Vpu-TM fits that of the WT complex very well. Thus, we aligned the representative structure of the mutant complex with the WT complex through fitting the Vpu-TM structure, and the alignment results are shown in Figure 5. Also, on the basis of the MD simulation trajectory, the binding energies for the mutant complexes were evaluated using the MMGBSA method, and the results are listed in Table 4.

Compared to the wild-type (WT) complex, the A14L or A18L Vpu mutant resulted in a significantly looser complex (Figure 5A), consistent with the results of the binding energy calculations [~3.75 or ~2.46 kcal/mol more disfavorable, respectively, than the WT complex (Table 4)]. Although this result suggested that both A14L and A18L mutations could disturb the Vpu–BST-2 interaction, calculations from per residue changes indicate that either one of the mutants may cause a benefit in the binding energy for the exact mutant residue but a penalty for the total complex. Thus, it is reasonable to propose that the A14L or A18L mutant may enhance the hydrophobic interaction of the exact residue with the BST2-TM motif, while the increase in the volume of the substitute residue may produce a steric clash, thus pushing BST2-TM away and weakening the interaction of the total. In contrast to the A14L and A18L mutants, the W22A mutant does not loosen the complex (Figure 5 A), while the mutant may cause penalties in the binding energy [3.61 kcal/mol for the exact mutant residue and 4.27 kcal/mol for the Vpu–BST-2 complex (Table 4)], indicating that the weak binding of the mutant residue to BST2-TM should account for the weakened interaction.

On the other hand, all of the I34A, L37A, and L41A mutations in BST2-TM could loosen the BST2-TM–Vpu-TM (Figure 5B), which is consistent with the binding energy calculation (Table 4). The per residue change calculations indicate that the mutant may cause a penalty in the binding energy for the exact mutant residue (Table 4.), which means the replacement of the residue may weaken the exact residue with Vpu-TM, and such a penalty for a single residue led to the relief of the overall interaction between the BST2-TM and Vpu-TM.

In general, our data show that all the mutants tested (Table 4) may cause disfavorable binding energy as a whole, which is consistent with the reported experimental data.[8,10] Thus, the results of the mutant analysis further validate the rationale of our binding mode. Notably, the binding mode we propose here does not consider the situation in which both Vpu and BST-2 may be prone to formation of an oligomer. Although the extracellular domain of BST-2 could form a parallel dimer via the disulfide linkage at C53, C63, and C91, it is thus far unclear whether the TMD of BST-2 could directly interact with itself. The TMD of Vpu likely forms a pentamer, and the polymerization of Vpu-TM is related to an ion channel activity.[38] It was reported that the ion channel activity of Vpu is dispensable for the Vpu-mediated downregulation of BST-2.[39] In addition, a small molecule, BIT225, was found to inhibit the ion channel activity but not affect the BST-2 antagonism of Vpu.[40] Together, these experimental facts suggest that the polymerization of Vpu might be dispensable for the interaction between Vpu and BST-2. Nevertheless, it is worthwhile to investigate in the future whether the polymerization of Vpu and a possible BST2-TM dimer could affect their interaction.

Interestingly, according to Kobiyashi's study,[10] the T45 mutation in Vpu caused the blockage of the Vpu-mediated antagonism of BST-2 with no effect on the interaction of BST-2 and Vpu. Although T45 was at the binding interface in our predicted binding mode, this residue, unlike I34, L37, and L41 at the interface, should have a much weaker interaction with the residues of Vpu because no residue atom of Vpu-TM was found


dx.doi.org/10.1021/bi2015986 | *Biochemistry* 2012, 51, 1288–1296

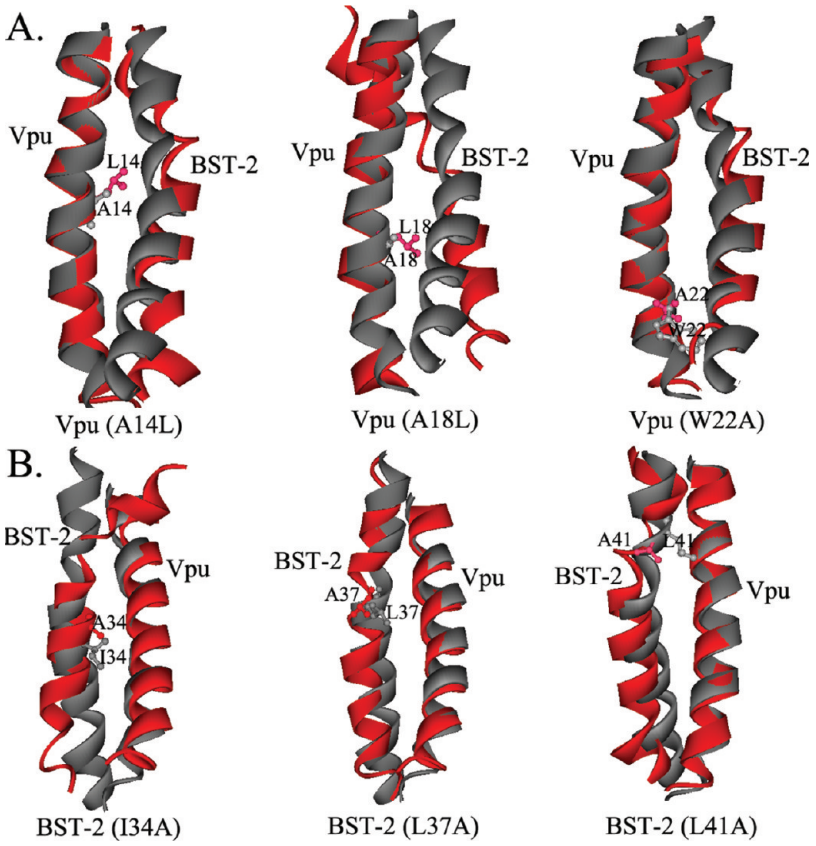


**Figure 5.** Results of molecular dynamics simulations of six mutant complex structures. The representative structure was generated by cluster analysis, and the alignment of the mutant complexes (red ribbons) with the wild-type complex (binding mode 1, gray ribbons) was conducted in DS. (A) Influence of the A14L, A18L, or W22A mutation in Vpu-TM on the Vpu−BST-2 interaction. (B) Influence of the I34A, L37A, or L41A mutation in BST2-TM on the Vpu−BST-2 interaction.

**Table 4. Binding Free Energy (kilocalories per mole) Evaluation for the Mutant Complexes**

| | $\Delta G_{gas}$ | $\Delta\Delta G_{gas}$ | $\Delta G_{bind}$ | $\Delta\Delta G_{bind}$ | $\Delta\Delta G_{single\ mutant}$ |
|---|---|---|---|---|---|
| WT | −69.09 ± 3.95 | 0.00 | −47.01 ± 3.23 | 0.00 | – |
| Vpu(A14L) | −39.61 ± 10.43 | 29.49 | −43.26 ± 2.94 | 3.75 | −0.96 |
| Vpu(A18L) | −51.01 ± 3.27 | 18.05 | −44.55 ± 3.10 | 2.46 | −0.30 |
| Vpu(W22A) | −54.44 ± 3.41 | 14.61 | −42.74 ± 3.18 | 4.27 | 3.61 |
| BST-2(I34A) | −51.64 ± 7.03 | 17.39 | −43.67 ± 3.11 | 3.34 | 2.49 |
| BST-2(I37A) | −66.77 ± 5.23 | 2.27 | −46.08 ± 3.11 | 0.93 | 0.23 |
| BST-2(L41A) | −48.13 ± 6.76 | 20.92 | −38.65 ± 3.61 | 8.36 | 1.12 |

within 5 Å of it. Thus, T45 should not act as a key residue for the interaction between Vpu and BST-2, and this may explain why a T45 mutation did not significantly affect the association of these two proteins. It remains unknown whether, in the antagonism of BST-2, some residues of Vpu-TM may play a direct or indirect role other than the involvement in the Vpu−BST-2 interaction, e.g., recruiting TrCP E3 ligase.

**Targeting the BST-2−Vpu Interface for Anti-HIV-1 Drug Discovery.** It has been proposed that blocking the Vpu-mediated downregulation process of BST-2 may provide a promising strategy in the treatment of HIV and AIDS.[1,13] Because the interaction between the BST2-TM dimer and the Vpu-TM dimer is critical for this process, the interface between BST-2 and Vpu becomes a potential target for anti-HIV drug development.[1,13] Mauricio proposed that the peptide decoy strategy, which has been successfully applied to design the anti-aIIb peptide via the CHAMPS (computed helical antimembrane protein) algorithm, would be a feasible way to design an inhibitor of the BST-2−Vpu interaction.[35] Specifically, overexpression of the TASK-1 TMD that is structurally homologous to Vpu inhibits Vpu-mediated enhancement of virion release.[41] On the other hand, our experimental data indicate that a peptide derived from the BST2-TM dimer increases the BST-2 level at the surface of HeLa-Vpu cells (Figure S5 of the Supporting Information). These lines of experimental evidence collectively support the rationale of an anti-HIV-1 drug targeting the BST-2−Vpu interface.

Although a peptide decoy might be a promising inhibitor for the BST-2 downregulation process, peptides are generally not suitable for drug development because of in vivo stability, pharmacokinetics, and bioavailability.[42] Therefore, the small molecules or peptidomimetic inhibitors of the Vpu-mediated BST-2 downregulation are strongly recommended. To rationally design the small inhibitors, knowledge of the binding mode is desired, to provide the detailed structural information for designing the pharmacophore. Herein, on the basis of our


dx.doi.org/10.1021/bi2015986 | *Biochemistry* 2012, 51, 1288−1296

binding mode, a pharmacophore was generated and is shown in Figure 6. Briefly, there are three hydrophobic features, which

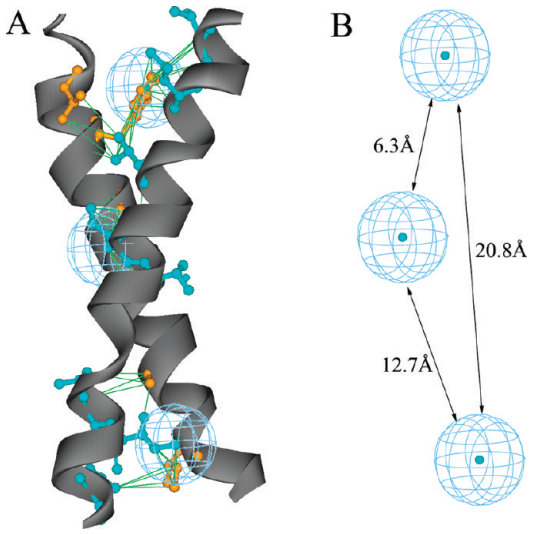


**Figure 6.** Generated pharmacophore based on the binding mode. (A) The pharmacophore was mapped to the complex structure (gray ribbons). (B) Geometric details of the pharmacophore feather (the hydrophobic feature is shown as blue spheres).

are mapped to the Trp22 and Val25 residues of Vpu-TM and the Leu23, Ile26, and Val30 residues of BST2-TM; the Ala14 and Ala18 residues of Vpu-TM and the Ile34 and Val35 residues of BST2-TM; and the Ala14 and Ala18 residues of Vpu-TM and the Ile6 and Val10 residues of BST2-TM (Figure 6A). The pharmacophore features constitute a triangle, and the length of each side between the pharmacophore features is 6.3, 12.7, or 20.8 Å. The pharmacophore provided the rather useful information for further rational drug design, and the virtual screen for the small molecule and the peptidomimetic design based on the pharmacophore is ongoing.

## CONCLUSION

In this work, a binding mode for the BST2-TM dimer and Vpu-TM dimer was generated through molecular modeling. The model is consistent with previous biological data, and further binding free energy evaluation of mutant complexes also supports the rationale of the binding mode. The binding mode gives an understanding of the interaction of the BST2-TM dimer and Vpu-TM dimer at the atomic level and will facilitate the development of an anti-HIV-1 drug targeting the interface of the BST-2–Vpu interaction.

## ASSOCIATED CONTENT

### Supporting Information

Details of molecular dynamic simulations (Table S1), a description of the model in a membrane (Figure S1), an alignment of the representative structure and the experimental structure for Vpu-TM (Figure S2), a comparison of the simulations in DOPC and POPC membranes of BST2-TM and Vpu-TM (Figure S3), the 50 ns simulation for BST-2 in a membrane and the alignment of the representative structures (Figure S4), and a bioassay of the BST2-TM dimer-derived peptide (Figure S5). This material is available free of charge via the Internet at http://pubs.acs.org.

## AUTHOR INFORMATION

### Corresponding Author

*J.Z.: e-mail, zhou_jim@hotmail.com; phone, 86-10-63131011. S.C.: e-mail, shancen@hotmail.com; phone, 86-10-63131011.

### Funding

This work was supported in part by the Natural Science Foundation of China (81001402), the National S&T Major Special Project on Major New Drug Innovation (2009ZX09303-005), and the National S&T International Collaboration (2010DFA31580 and 2010DFB30870).

### Notes

The authors declare no competing financial interest.

## ACKNOWLEDGMENTS

We thank Dr. R. C. Rizzo at Stony Brook University (Stony Brook, NY) for discussions concerning the calculation of binding free energies. We also thank Dr. Lawrence Kleiman at Lady Davis Institute of McGill University for help with the language of the manuscript.

## REFERENCES

(1) Kuhl, B. D., Cheng, V., Wainberg, M. A., and Liang, C. (2011) Tetherin and Its Viral Antagonists. *J. Neuroimmune Pharmacol. 6*, 188–201.

(2) Neil, S. J., Zang, T., and Bieniasz, P. D. (2008) Tetherin inhibits retrovirus release and is antagonized by HIV-1 Vpu. *Nature 451*, 425–430.

(3) Zhang, J. Y., and Liang, C. (2010) BST-2 Diminishes HIV-1 Infectivity. *J. Virol. 84*, 12336–12343.

(4) Dube, M., Roy, B. B., Guiot-Guillain, P., Binette, J., Mercier, J., Chiasson, A., and Cohen, E. A. (2010) Antagonism of Tetherin Restriction of HIV-1 Release by Vpu Involves Binding and Sequestration of the Restriction Factor in a Perinuclear Compartment. *PLoS Pathog. 6*, e100865.

(5) Douglas, J. L., Viswanathan, K., McCarroll, M. N., Gustin, J. K., Fruh, K., and Moses, A. V. (2009) Vpu Directs the Degradation of the Human Immunodeficiency Virus Restriction Factor BST-2/Tetherin via a $\beta$ TrCP-Dependent Mechanism. *J. Virol. 83*, 7931–7947.

(6) Maldarelli, F., Chen, M.-Y., Willey, R. L., and Strebel, K. (1993) Human Immunodeficiency Virus Type 1 Vpu Protein Is an Oligomeric Type I Integral Membrane Protein. *J. Virol. 67*, 5056–5061.

(7) Rong, L., Zhang, J., Lu, J., Pan, Q., Lorgeoux, R. P., Aloysius, C., Guo, F., Liu, S.-L., Wainberg, M. A., and Liang, C. (2009) The Transmembrane Domain of BST-2 Determines Its Sensitivity to Down-Modulation by Human Immunodeficiency Virus Type 1 Vpu. *J. Virol. 83*, 7536–7546.

(8) Vigan, R., and Neil, S. J. (2010) Determinants of Tetherin Antagonism in the Transmembrane Domain of the Human Immunodeficiency Virus Type 1 Vpu Protein. *J. Virol. 84*, 12958–12970.

(9) McNatt, M. W., Zang, T., Hatziioannou, T., Bartlett, M., Ben Fofana, I., Johnson, W. E., Neil, S. J., and Bieniasz, P. D. (2009) Species-Specific Activity of HIV-1 Vpu and Positive Selection of Tetherin Transmembrane Domain Variants. *PLoS Pathog. 5*, e100300.

(10) Kobayashi, T., Ode, H., Yoshida, T., Sato, K., Gee, P., Yamamoto, S. P., Ebina, H., Strebel, K., Sato, H., and Koyanagi, Y. (2011) Identification of Amino Acids in the Human Tetherin Transmembrane Domain Responsible for HIV-1 Vpu Interaction and Susceptibility. *J. Virol. 85*, 932–945.

(11) Tervo, H. M., Homann, S., Ambiel, I., Fritz, J. V., Fackler, O. T., and Keppler, O. T. (2011) $\beta$-TrCP is dispensable for Vpu's ability to overcome the CD317/Tetherin-imposed restriction to HIV-1 release. *Retrovirology 8*, 9.

(12) Sauter, D., Specht, A., and Kirchhoff, F. (2010) Tetherin: Holding On and Letting Go. *Cell 141*, 392–398.

(13) Tokarev, A., Skasko, M., Fitzpatrick, K., and Guatelli, J. (2009) Antiviral Activity of the Interferon-Induced Cellular Protein BST-2/Tetherin. *AIDS Res. Hum. Retroviruses 25*, 1197−1210.
(14) Paul, M., Mazumder, S., Raja, N., and Jabbar, M. A. (1998) Mutational Analysis of the Human Immunodeficiency Virus Type 1 Vpu Transmembrane Domain That Promotes the Enhanced Release of Virus-Like Particles from the Plasma Membrane of Mammalian Cells. *J. Virol. 72*, 1270−1279.
(15) Schubert, U., Bour, S., Ferrer-Montiel, A. V., Montal, M., Maldarell, F., and Strebel, K. (1996) The two biological activities of human immunodeficiency virus type 1 Vpu protein involve two separable structural domains. *J. Virol. 70*, 809−819.
(16) Tiganos, E., Friborg, J., Allain, B., Daniel, N. G., Yao, X.-J., and Cohen, E. A. (1998) Structural and Functional Analysis of the Membrane-Spanning Domain of the Human Immunodeficiency Virus Type 1 Vpu Protein. *Virology 251*, 96−107.
(17) Jia, B., Serra-Moreno, R., Neidermyer, W., Rahmber, A., Mackey, J., Fofana, I. B., Johnson, W. E., Westmoreland, S., and Evans, D. T. (2009) Species-specific activity of SIV Nef and HIV-1 Vpu in overcoming restriction by tetherin/BST2. *PLoS Pathog. 5*, e1000429.
(18) Gupta, R. K., Hué, S., Schaller, T., Verschoor, E., Pillay, D., and Towers, G. J. (2009) Mutation of a Single Residue Renders Human Tetherin Resistant to HIV-1 Vpu-Mediated Depletion. *PLoS Pathog. 5*, e1000443.
(19) Park, S. H., Mrse, A. A., Nevzorov, A. A., Mesleh, M. F., Oblatt-Montal, M., Montal, M., and Opella, S. J. (2003) Three-dimensional structure of the channel-forming trans-membrane domain of virus protein "u" (Vpu) from HIV-1. *J. Mol. Biol. 333*, 409−424.
(20) Zhao, T. X., Martinko, A. J., Le, V. H., Zhao, J., and Yin, H. (2010) Development of Agents that Modulate Protein-Protein Interactions in Membranes. *Curr. Pharm. Des. 16*, 1055−1062.
(21) Yin, H., Slusky, J. S., Berger, B. W., Walters, R. S., Vilaire, G., Litvinov, R. I., Lear, J. D., Caputo, G. A., Bennett, J. S., and DeGrado, W. F. (2007) Computational design of peptides that target transmembrane helices. *Science 315*, 1817−1822.
(22) McGillick, B. E., Balius, T. E., Mukherjee, S., and Rizzo, R. C. (2010) Origins of Resistance to the HIVgp41 Viral Entry Inhibitor T20. *Biochemistry 49*, 3575−3592.
(23) Lopez, C. F., Montal, M., Blasie, J. K., Klein, M. L., and Moore, P. B. (2002) Molecular dynamics investigation of membrane-bound bundles of the channel-forming transmembrane domain of viral protein U from the human immunodeficiency virus HIV-1. *Biophys. J. 83*, 1259−1267.
(24) Moore, P. B., Zhong, Q. F., Husslein, T., and Klein, M. L. (1998) Simulation of the HIV-1 Vpu transmembrane domain as a pentameric bundle. *FEBS Lett. 431*, 143−148.
(25) Candler, A., Featherstone, M., Ali, R., Maloney, L., Watts, A., and Fischer, W. B. (2005) Computational analysis of mutations in the transmembrane region of Vpu from HIV-1. *Biochim. Biophys. Acta 1716*, 1−10.
(26) Ulmschneider, J. P., and Ulmschneider, M. B. (2007) Folding Simulations of the Transmembrane Helix of Virus Protein U in an Implicit Membrane Model. *J. Chem. Theory Comput. 3*, 2335−2346.
(27) Krüger, J., and Fischer, W. B. (2009) Assembly of Viral Membrane Proteins. *J. Chem. Theory Comput. 5*, 2503−2513.
(28) Skasko, M., Tokarev, A., Chen, C., Fischer, W. B., Pillai, S. K., and Guatelli, J. (2011) BST-2 is rapidly down-regulated from the cell surface by the HIV-1 protein Vpu: Evidence for a post-ER mechanism of Vpu-action. *Virology 411*, 65−77.
(29) Skasko, M., Wang, Y., Tian, Y., Tokarev, A., Munguia, J., Ruiz, A., Stephens, E. B., Opella, S. J., and Guatelli, J. (2012) HIV-1 Vpu antagonizes the innate restriction factor BST-2 via lipid-embedded helix-helix interactions. *J. Biol. Chem. 287*, 58−67.
(30) Humphrey, W., Dalke, A., and Schulten, K. (1996) VMD: Visual molecular dynamics. *J. Mol. Graphics 14*, 33−38.
(31) Feller, S. E., Zhang, Y. H., Pastor, R. W., and Brooks, B. R. (1995) Constant-pressure molecular-dynamics simulation: The langevin piston method. *J. Chem. Phys. 103*, 4613−4621.
(32) Kollman, P. A., Massova, I., Reyes, C., Kuhn, B., Huo, S., Chong, L., Lee, M., Lee, T., Duan, Y., Wang, W., Donini, O., Cieplak, P., Srinivasan, J., Case, D. A., and Cheatham, T. E. III (2000) Calculating Structures and Free Energies of Complex Molecules: Combining Molecular Mechanics and Continuum Models. *Acc. Chem. Res. 33*, 889−897.
(33) Onufriev, A., Case, D. A., and Bashford, D. (2002) Effective Born radii in the generalized Born approximation: The importance of being perfect. *J. Comput. Chem. 23*, 1297−1304.
(34) Weiser, J., Shenkin, P. S., and Still, W. C. (1999) Approximate atomic surfaces from linear combinations of pairwise overlaps (LCPO). *J. Comput. Chem. 20*, 217−230.
(35) Montal, M. (2009) Vpu Matchmakers as a Therapeutic Strategy for HIV Infection, Plos. *Pathogens 5*, e100246.
(36) Lula, R., and Ian, R. G. (2008) Structure and Dynamics of Phospholipid Bilayers Using Recently Developed General All-Atom Force Fields. *J. Comput. Chem. 29*, 24−37.
(37) Jójárt, B., and Martinek, T. A. (2007) Performance of the General Amber Force Field in Modeling Aqueous POPC Membrane Bilayers. *J. Comput. Chem. 28*, 2051−2058.
(38) Mehnert, T., Lam, Y. H., Judge, P. J., Routh, A., Fischer, D., Watts, A., and Fischer, W. B. (2007) Towards a mechanism of function of the viral ion channel Vpu from HIV-1. *J. Biomol. Struct. Dyn. 24*, 589−596.
(39) Bolduan, S., Votteler, J., Lodermeyer, V., Greiner, T., Koppensteiner, H., Schindler, M., Thiel, G., and Schubert, U. (2011) Ion channel activity of HIV-1 Vpu is dispensable for counteraction of CD317. *Virology 416*, 75−85.
(40) Kuhl, B. D., Cheng, V., Donahue, D. A., Sloan, R. D., Liang, C., Wilkinson, J., and Wainberg, M. A. (2011) The HIV-1 Vpu Viroporin Inhibitor BIT225 Does Not Affect Vpu-Mediated Tetherin Antagonism. *PLoS One 6*, e27660.
(41) Hsu, K., Seharaseyon, J., Dong, P., Bour, S., and Marbán, E. (2004) Mutual Functional Destruction of HIV-1 Vpu and Host TASK-1 Channel. *Mol. Cell 14*, 259−267.
(42) Grdisa, M. (2011) The Delivery of Biologically Active (Therapeutic) Peptides and Proteins into Cells. *Curr. Med. Chem. 18*, 1373−1379.